RSC Advances

PAPER

View Article Online
View Journal | View Issue

Check for updates

Cite this: *RSC Adv.*, 2024, **14**, 13017

High performance electrochemical CO_2 reduction over Pd decorated cobalt containing nitrogen doped carbon†

Shayan Gul,[a] Fatima Nasim,[a] Waheed Iqbal,[a] Amir Waseem[a] and Muhammad Arif Nadeem *[ab]

Efficient electrocatalytic CO_2 reduction reaction (eCO_2RR) to various products, such as carbon monoxide (CO), is crucial for mitigating greenhouse gas emissions and enabling renewable energy storage. In this article, we introduce Pd nanoparticles which are deposited over in-house synthesized nitrogen doped tubular carbon (NC) whose ends are blocked with cobalt oxide (CoOx). This composite material is denoted as Pd@CoOx/NC. Among the series of synthesized electrocatalysts, the optimum ratio (Pd@CoOx/NC1) within this category exhibits exceptional performance, manifesting an 81% faradaic efficiency (FE) for CO generation which was quantitatively measured using a gas chromatograph. This remarkable efficiency can be attributed to several scientific factors. Firstly, the presence of Pd nanoparticles provides active sites for CO_2 reduction. Secondly, the NC offer enhanced electrical conductivity and facilitate charge transfer during the reaction. Thirdly, the CoOx capping at the ends of the NC serves to stabilize the catalyst, favoring the formation of CO. The remarkable selectivity of the catalyst is further confirmed by the qualitative CO detection method using $PdCl_2$ strips. Pd@CoOx/NC1 exhibits a high current density of 55 mA cm^{-2} and a low overpotential of 251 mV, outperforming Pd decorated multiwalled carbon nanotubes (Pd@MWCNTs) which shows a higher overpotential of 481 mV. Pd@CoOx/NC1 shows long-term stability at different potentials and rapid reaction kinetics. These findings highlight Pd@CoOx/NC1 as promising CO_2 reduction catalysts, with implications for sustainable energy conversion techniques.

Received 2nd March 2024
Accepted 15th April 2024

DOI: 10.1039/d4ra01641f

rsc.li/rsc-advances

Open Access Article. Published on 23 April 2024. Downloaded on 1/17/2026 12:32:28 AM.
This article is licensed under a Creative Commons Attribution-NonCommercial 3.0 Unported Licence.

Introduction

The exploration of renewable energy sources to circumvent the adverse environmental effects of fossil fuels is a hot topic of research nowadays.[1–4] Among the different fuel cell technologies, the reduction of carbon dioxide is the most appealing as the rising CO_2 concentration in the atmosphere has caused serious environmental concerns.[5–9] Electrocatalytic CO_2 reduction reaction (eCO_2RR) is the most attractive route because of the efficient energy storage and conversion techniques.[10] The pathway of eCO_2RR can usually be divided into four basic steps, including (1) CO_2 adsorption; (2) CO_2 activation; (3) product formation; (4) product desorption.[11] The CO production requires only two proton coupled electron transfer (PCET) steps. The 1st PCET step is $* + CO_2 + H^+ + e^- \rightarrow *COOH$, and 2nd PCET step is $*COOH + H^+ + e^- \rightarrow * + CO + H_2O$.[12] The development of low-cost and efficient catalyst is highly desirable to address several challenges associated with eCO_2RR such as high overpotential (η), limited FE, slow kinetics due to multistep electron transfer, and competitive hydrogen evolution reaction (HER).[13,14] Palladium has been well known for its excellent ability to convert CO_2 to CO with a high degree of selectivity (up to 90%), where both products have their marketplace and economic viability.[15] The strong binding energies of C-bound intermediates (*CO and *COOH *etc.*) on the Pd, leading to CO_2 activation and suppression of competitive HER with impressive FEs at low η makes it a highly desirable candidate to be used in eCO_2RR.[16]

For example, Hori *et al.* reported CO production by using crystalline Pd foil with FE of 28% at -0.8 V_{RHE}.[17] Similarly, Gao *et al.* conducted size-based investigations on palladium nanoparticles and observed a remarkably high FE of 91.2% for CO at -0.89 V_{RHE}.[10] Sheng *et al.* reported noteworthy FE for CO production ~40% at $-0.6V_{RHE}$ for Pd/C electrocatalyst.[18] These findings revealed that the eCO_2RR abilities of Pd foil, Pd NPs, and Pd/C catalysts are limited due to their smaller surface areas, particle agglomeration, and carbon corrosion. Furthermore, Pd faces the challenge of CO-poisoning which decreases the CO production rate during eCO_2RR.[19] A proficient approach to

[a]*Catalysis and Nanomaterials Lab 27, Department of Chemistry, Quaid-i-Azam University, Islamabad 45320, Pakistan. E-mail: manadeem@qau.edu.pk*

[b]*Pakistan Academy of Sciences, 3-Constitution Avenue Sector G-5/2, Islamabad, Pakistan*

† Electronic supplementary information (ESI) available. See DOI: https://doi.org/10.1039/d4ra01641f

© 2024 The Author(s). Published by the Royal Society of Chemistry

Open Access Article. Published on 23 April 2024. Downloaded on 1/17/2026 12:32:28 AM. This article is licensed under a Creative Commons Attribution-NonCommercial 3.0 Unported Licence.

address these challenges associated with eCO_2RR involves a systematic sequence of CO_2 adsorption,[20–22] intermediate formation,[23,24] and product removal[25,26] on active sites during the electrocatalytic reaction.

The combination of Pd with other metals greatly lowers the CO binding strength by tuning the electronic properties of Pd, leading to facile desorption which in turn increases its production.[27] For example, Yin *et al.* reported improved CO current density on the surface of CuPd NPs with FE_{CO} ~86%.[28] Similarly, AgPd NPs have been shown to alleviate the CO poisoning of Pd without scarifying the FE_{CO}.[27]

The pyrolysis of metal organic frameworks (MOF), an ideal precursor for the synthesis of carbon based materials, yields high surface area carbon with a metal oxide or metal nanoparticles disseminated or encapsulated within the ligand-derived matrix.[29] The presence of metal within the porous carbon derived from MOF imparts stability and prevents the leaching of carbon during the electrocatalytic process.[3,30] MOF derived carbon promotes fast electron transfer and provides redox active sites due to the presence of heteroatoms. These properties make MOF an attractive candidate to be used as a matrix for the uniform dispersion of metal nanoparticles.[29] Xi *et al.* synthesized Fe–N_4 sites from Fe doped MOF precursor (ZIF-8). The material exhibited electrocatalytic activity towards CO_2RR with FE ~86.9%.[31] Likewise, Wang and co-workers reported nearly 100% FE at −0.9 V_{RHE} for Fe–N–C sites.[32]

Doping of heteroatoms that have different electronegativities (like; B, N, and P) plays a pivotal role in eCO_2RR.[33,34] In the realm of heteroatom doping, nitrogen (N) stands out as the most common dopant utilized. Meyer *et al.* documented the synthesis of nitrogen-doped carbon nanotubes (NCNTs) to enhance the selectivity of eCO_2RR towards formate production, achieving an efficiency of 59%.[22] Zhou *et al.* reported that relative to pristine CNTs, graphitic and pyridinic N-containing CNTs enhance the eCO_2RR towards CO with lower η (−0.18 V) and higher FE_{CO} (80%).[35] In the context of eCO_2RR, CO_2 molecules are initially adsorbed onto basic N-binding sites. Subsequent reduction leads to the formation of $*CO_2^{\bullet-}$ anion radicals. These stabilized $*CO_2^{\bullet-}$ species play a pivotal role in enhancing both activity and selectivity.[36]

Keeping in view the aforementioned properties, herein we have synthesized cobalt oxide incorporated nitrogen doped tubular carbon (CoOx/NC) originated from zeolitic imidazolate framework-12 (ZIF-12). ZIF-12 contains cobalt ions coordinated with benzimidazolate ligands $[Co(PhIM)_2]_n$, exhibiting a metal atom density of 2.01 nm^{-3}. With a diameter capacity of 14.64 Å, its largest cage comprises 48 vertices.[37] The extraordinary porosity and stability of ZIF-12 make it an ideal precursor for synthesizing CoOx/NCs with tailored properties. The synthesized CoOx/NC was decorated with palladium nanoparticles by sodium borohydride ($NaBH_4$) reduction technique. The synthesized cost-effective catalysts (Pd@CoOx/NCs) were found to be active for eCO_2RR with significant FE_{CO}. The Pd nanoparticles provide active sites for CO_2 reduction, whereas NCs enhance electrical conductivity, facilitating rapid charge transfer during the reaction, and the CoOx capping at the tubular carbon ends stabilizes the catalyst and may selectively influence the reaction pathway, ultimately promoting CO formation. The CoOx/NC prevents the agglomeration of Pd NPs during the reduction process, making it a highly efficient, antipoisoning, stable, and selective catalyst towards eCO_2RR. The method presented here is facile and does not involve multisteps. The effect of CoOx on the Pd NPs for eCO_2RR has not been observed yet to the best of our knowledge. This innovative idea solves the challenge of using Pd, a well-known catalyst for CO_2 reduction, benefiting from the properties of CoOx/NC. The concentration effect of palladium on the reduction of CO_2 was examined by synthesizing a novel series of electrocatalysts with varied palladium concentrations (Pd@CoOx/NCs). The optimized electrocatalyst (Pd@CoOx/NC1) delivered maximum current density (j) with high selectivity for CO.

Palladium chloride ($PdCl_2$) strips, a unique and incredibly efficient technique, were used to qualitatively detect CO gas produced during CO_2 reduction. By offering a simple and accurate way to identify and confirm the presence of CO, this novel approach represents a significant improvement in the discipline of chemistry. The method relies on the distinctive color change exhibited by the $PdCl_2$ strips, facilitating easy visual detection of CO. Its simplicity, accuracy, and reliability make it an invaluable tool for CO detection in various chemical reactions.

Experimental

Synthesis of ZIF-12

For the synthesis of ZIF-12, two solutions were made. Solution A contains 1.3 mmol of cobalt nitrate hexahydrate ($Co(NO_3)_2 \cdot 6H_2O$) dispersed in 7 mL of *N*,*N*-Dimethyl formamide (DMF). Solution B contains 6 mmol of benzimidazole ($C_7H_6N_2$) dissolved in 7 mL of DMF. Both the solutions were mixed, transferred to a Teflon-lined autoclave, and placed in an oven at 150 °C for 48 h. The product obtained was collected and subsequently washed several times with deionized (DI) water and DMF to ensure the removal of any residual impurities.

Synthesis of CoOx/NC

ZIF-12 was subjected to a well-controlled carbonization process at high temperatures in an Argon (Ar) atmosphere to synthesize the support material (CoOx/NC). To accomplish this, 200 mg of ZIF-12 was carefully placed inside a tube furnace. To remove traces of oxygen gas, the tube furnace was subjected to degassing for a period of 2 h with a continuous flow of Ar. After the degassing procedure, the system was gradually raised to 850 °C at 5 °C per minute and kept for 8 h. The synthesized material was carefully collected after natural cooling to room temperature. High-purity HCl was used to treat the synthesized product to remove any remaining cobalt species and improve the surface functionalities. This treatment aimed to increase both the adsorption capacity and dispensability of the material. After completion of the acid leaching process, the material showed a cobalt content of roughly 2.2 wt%, according to extensive X-ray photoelectron spectroscopy (XPS) and atomic absorption spectroscopy (AAS) analysis.

© 2024 The Author(s). Published by the Royal Society of Chemistry

Open Access Article. Published on 23 April 2024. Downloaded on 1/17/2026 12:32:28 AM. This article is licensed under a Creative Commons Attribution-NonCommercial 3.0 Unported Licence.

Synthesis of Pd@CoOx/NC catalysts

The catalyst was synthesized by a previously reported method.[30] To synthesize the catalysts, 70 mg of CoOx/NC were dispersed in DMF by sonication for 60 min. After that, the mixture underwent a precise dropwise addition of a 5% palladium diacetate solution (20 mg) and was sonicated for further 30 min. After that sodium borohydride (2 mg mg^{-1} of metal salt) was added. The whole mixture then underwent a 30 min sonication process, followed by stirring at 60 °C for an additional 30 min. The product was cooled, filtered, and then extensively washed with DMF and methanol. To investigate the concentration effect, various catalysts were synthesized by altering the amount of precursor metal salt. The electrocatalyst loading for Pd@CoOx/NC1, Pd@CoOx/NC2, and Pd@CoOx/NC3 was determined to be 0.02242 mg_{Pd} cm^{-2}, 0.016815 mg_{Pd} cm^{-2}, and 0.01273 mg_{Pd} cm^{-2}, respectively. The electrochemical activities of these catalysts were then examined to investigate the effect of concentration. In Scheme 1, a detailed description of the synthesis of Pd@CoOx/NCs is provided.

Electrochemical measurements

All CO_2 electrochemical studies were carried out using GAMRY Interface 5000 E electrochemical workstation in conjugation with gas-tight H-cell equipment with a proton exchange membrane (PEM; Nafion 117) as a partition between the cathodic and anodic compartments. The cathodic chamber houses the glassy carbon as a working electrode where the CO_2 reduction process takes place. To ensure precise potential control, an Ag/AgCl reference electrode was employed, along with a counter electrode *i.e.*, graphitic rod (Fig. S6†). The working electrode with the catalyst coating is made by dispersing 3 mg of the synthesized catalyst in a solution of 80 μL isopropanol and 20 μL of a 5% Nafion. Using the drop casting technique, a glassy carbon electrode was deposited with the homogenized slurry, ensuring an even and consistent coating. This electrochemical analysis carried out in 0.1 M $KHCO_3$ electrolyte solution (pH 6.8) provided insights into the catalyst's activity, kinetics, and stability. All measurements were carried out under ambient conditions *i.e.*, atmospheric pressure and room temperature. For eCO_2RR product analysis, a 500 μL gas sample from the cathode chamber was extracted and injected into a gas chromatograph. The gas chromatograph featured a thermal conductivity detector (TCD) for precise quantitative gaseous product (CO) analysis.

Results and discussion

Powder X-ray diffraction (PXRD) analysis was carried out to investigate the crystalline structure, elemental composition, and phase purity of the sample. Cubic crystal structure, with the $Fm\bar{3}m$ space group was exhibited by palladium metal in the synthesized materials. PXRD of all the synthesized materials has been shown in Fig. 1a. The distinguished peak observed at 2θ value of 25.81°, attributed to the (002) plane of graphitic carbon, provides strong evidence for the consistent presence and persistence of graphitic carbon across all the synthesized catalysts. The presence of graphitic carbon is further supported by the identification of two additional peaks at 2θ values of ~44.41° and ~51.51° (Fig. 1a), which are aligned with the distinctive pattern documented in the JCPDS card no. 00-013-0148. Due to the low cobalt content (*ca.* 2 wt%), as found by XPS investigations, the XRD peaks for cobalt oxide (CoOx) have not appeared. However, investigations using high-resolution transmission electron microscopy (HRTEM), XPS, and selected area electron diffraction (SAED) clearly show that CoOx nanoparticles exist.[38] The formation of palladium nanoparticles was confirmed by the presence of diffraction rays at 2θ ~39.61°, ~44.21°, and ~68. 11°.

Table S1† displays the determined cell parameters (*a*) and the associated *d*-spacing values obtained for crystallographic planes of Pd ((220), (200), and (111)) by the application of Bragg's law. These calculated results demonstrate a high level of concurrence and conformity with the observations derived from HRTEM analysis. A slight increase in the lattice parameter '*a*' and *d*-spacing is noticeable in the synthesized materials compared to fcc-type Pd nanoparticles (Table S1†). This deviation can be attributed to the electronic interaction between palladium and cobalt, resulting in lattice growth. The obtained values indicate metal strain and lattice distortion in the synthesized electrocatalysts, exhibiting a synergistic effect. PXRD of MWCNTs and Pd@MWCNTs has been presented in Fig. S1.†

XPS was utilized to investigate the surface elemental composition, oxidation state, and electronic properties of the optimized electrocatalyst Pd@CoOx/NC1 (Fig. 1). The Co 2p spectrum exhibits a peak for the presence of metallic cobalt at 777.8 eV. The observed peaks at 781.2 eV and 796.9 eV relate to Co $2p_{3/2}$ and Co $2p_{1/2}$, respectively indicating the cobalt

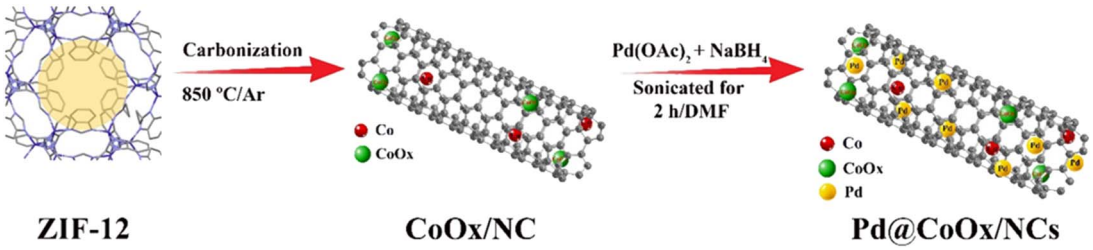

Scheme 1 Schematic illustration of the fabrication of Pd@CoOx/NCs.

Open Access Article. Published on 23 April 2024. Downloaded on 1/17/2026 12:32:28 AM.
This article is licensed under a Creative Commons Attribution-NonCommercial 3.0 Unported Licence.

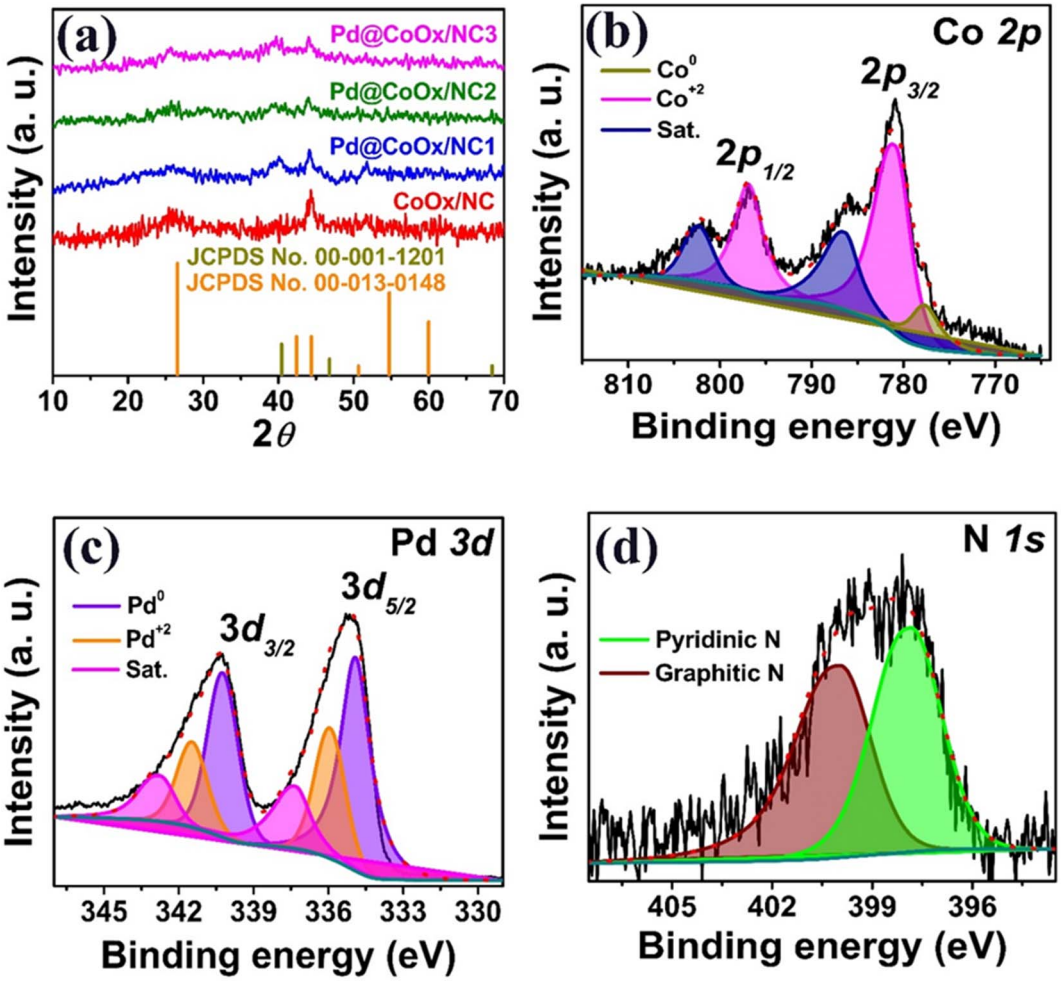

Fig. 1 (a) PXRD of all the synthesized electrocatalysts along their JCPDS. XPS data of Pd@CoOx/NC1 (b) Co 2p (c) Pd 3d (d) N 1s.

oxidation within the support material (Fig. 1b).[38] In Fig. 1c, the XPS spectrum of Pd nanoparticles displays two distinct peaks at 334.8 eV (Pd $3d_{5/2}$) and 340.2 eV (Pd $3d_{3/2}$). These values indicate that palladium primarily exists in the metallic state. The negative shift in palladium metal binding energy (standard value ~335 eV) is an indication of electron transfer from cobalt species, resulting in a distinct electronic environment around palladium and a downward shift in its d-band center relative to the Fermi level. The electronegative nature of palladium (E. N ~2.20) caused the extraction of electrons from cobalt (E. N ~1.88), which in turn decreased the energy of palladium d-band center due to the increased valence charge on the palladium center.[30,39] The observed findings were aligned with the d-band center model, as the palladium metal undergoes a downward shift of its d-band to compensate for the distortion caused by the electronic interaction with cobalt. The two distinct peaks revealed in the high-resolution profile of N 1s at 397.8 eV and 400 eV correspond to pyridinic nitrogen and graphitic nitrogen, respectively (Fig. 1d).[38] The high-resolution O 1s spectrum exhibits three peaks at binding energies of 531.3 eV, 533.6 eV, and 535.9 eV, corresponding to oxygen bonded to the metal and surface-bound oxygen species, respectively (Fig. S2a†).[38]

The deconvolution of the C 1s core level spectrum revealed four peaks. The peaks at binding energies of 284.2 eV and 286 eV correspond to sp^2 (C=C) and sp^3 (C–C) hybridized carbon, respectively. The remaining peaks at 288.1 eV and 289.4 eV arise from surface-bound oxygen groups (Fig. S2b†).[38,40] The XPS analysis of CoOx/NC is presented in Fig. S4.†

HRTEM analysis (Fig. 2) provided a detailed analysis of morphology and structure and showed the presence of distinct cylindrical tubes encapsulating cobalt oxide (CoOx) nanoparticles. CoOx nanoparticles, with a size of approximately 50 nm, are localized at the terminals of NC (Fig. S5†). Upon closer examination of the NC structure, the nanoparticles are observed to be encapsulated within layers of tubular carbon. The tubes exhibit distinct curved growth lines, uniformly bending in the same direction to one another. Growth lines developed as curved layers emanating from the surface of the nanoparticles exhibit a non-concentric configuration (Fig.-S5b†). The existence of oxygen and nitrogen heteroatoms in the precursor material promotes carbon condensation at elevated temperatures, leading to the formation of a highly interconnected matrix of tubular carbon with intertwined nodes and internodes. The interconnected nodes are supposed to serve as

© 2024 The Author(s). Published by the Royal Society of Chemistry

Open Access Article. Published on 23 April 2024. Downloaded on 1/17/2026 12:32:28 AM.
This article is licensed under a Creative Commons Attribution-NonCommercial 3.0 Unported Licence.

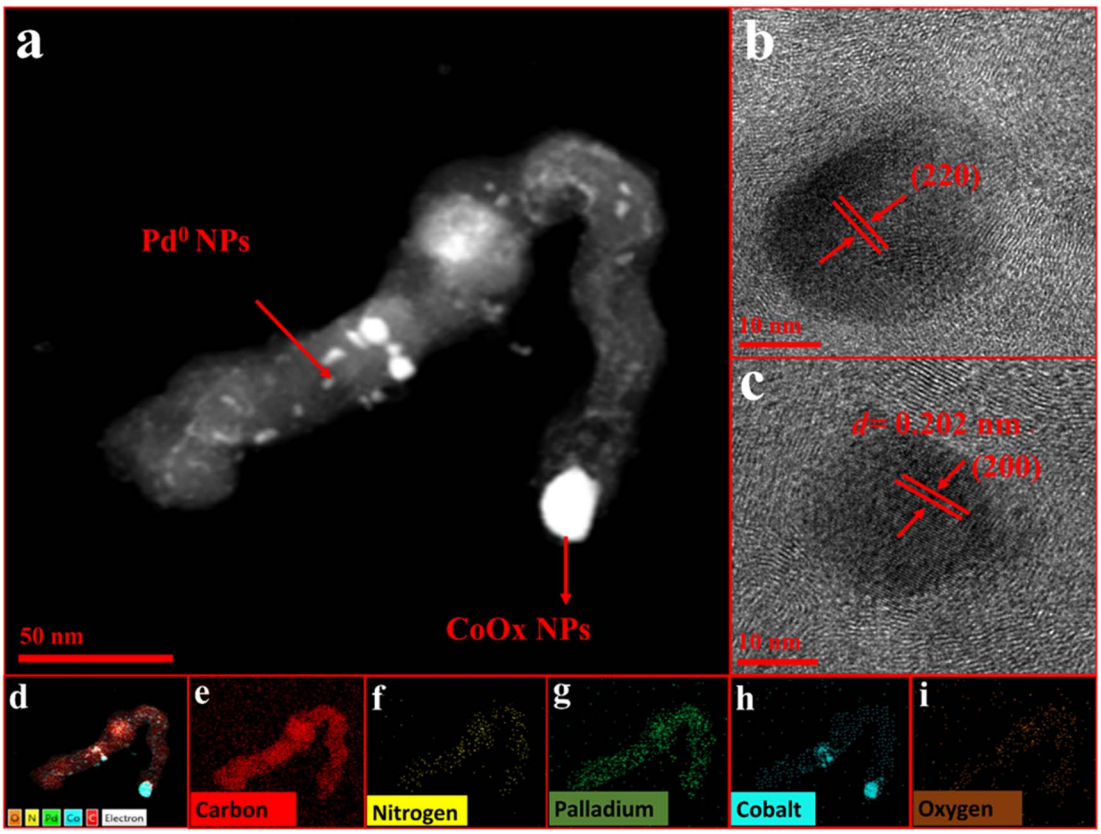

Fig. 2 (a) HRTEM analysis of Pd@CoOx/NC1 (a) 50 nm (b and c) 10 nm (d) elemental mapping of Pd@CoOx/NC1 (e) C (f) N (g) Pd (h) Co (i) O.

anchoring sites for the loaded palladium metal nanoparticles, facilitating their immobilization (Fig. S5†). Elemental mapping of Pd@CoOx/NC1 analysis provides conclusive evidence of the presence of cobalt, nitrogen, oxygen, palladium, and carbon within the sample (Fig. 2d–i). Nanoparticles of palladium, characterized by their spherical morphology, exhibit homogeneous dispersion within NC, which also contains embedded CoOx.

The results obtained deliver conclusive evidence that palladium nanoparticles were successfully deposited onto the CoOx/NC framework. The HRTEM analysis undoubtedly demonstrates the presence of distinct fringes corresponding to the loaded nanoparticles (Fig. 2b and c). The fringes detected in the HRTEM analysis correspond to specific crystallographic planes of the palladium nanoparticles, with *d*-spacing values of 0.138 nm and 0.204 nm attributed to the (220) and (200) planes, correspondingly. HRTEM analysis findings are aligned with the XRD results presented in Table S1.† Additionally, the EDX pattern of Pd@CoOx/NC1 has been depicted in Fig S3,† which provides further supporting evidence for the deposition of palladium nanoparticles.

Electrochemical investigations

Linear sweep voltammetry (LSV) measurements were performed in 0.1 M $KHCO_3$ electrolytes saturated with both Ar and CO_2. The experiments were conducted at 10 mV s^{-1}. Response of Pd@MWCNTs exhibited a significant contrast when exposed to Ar and CO_2 atmospheres. Under CO_2 saturated conditions, it exhibited a high overpotential of 481 mV and a very low value of j ~6 mA cm^{-2} for CO_2 reduction. Conversely, in the Ar medium, no discernible reduction peak was observed, resulting in a lower j of 2 mA cm^{-2} (Fig. 3a). Similarly, Pd@CoOx/NC1 also exhibited an absence of reduction peaks in the Ar medium, yielding a current density of 15 mA cm^{-2}. However, following 1 h CO_2 purging, Pd@CoOx/NC1 demonstrated outstanding performance. It exhibited a remarkably low overpotential of 251 mV, signifying enhanced catalytic activity, accompanied by a significantly higher current density of 55 mA cm^{-2} (Fig. 3b). The remarkable performance of Pd@CoOx/NC1 as a catalyst for CO_2 reduction reactions unequivocally demonstrates its superior CO_2 electrocatalytic capabilities. Amongst all the electrocatalysts examined, Pd@CoOx/NC1 shows the most favorable CO_2 reduction performance at notably lower η. In the CO_2-saturated medium, the recorded current densities for all the synthesized electrocatalysts are in the following order: MWCNTs (2 mA cm^{-2}) < CoOx/NC (5 mA cm^{-2}) < Pd@MWCNTs (6 mA cm^{-2}) < Pd@CoOx/NC3 (18 mA cm^{-2}) < Pd@CoOx/NC2 (28 mA cm^{-2}) < Pd@CoOx/NC1 (55 mA cm^{-2}). The higher electrocatalytic activity of Pd@CoOx/NCs compared to Pd@MWCNTs towards eCO_2RR indicates the role of CoOx. The results of the partial current density for CO are illustrated in (Fig. 3d). These results highlight the superior electrocatalytic activity of Pd@CoOx/NC1, which is confirmed by its larger current density in comparison to the other catalysts being studied.

© 2024 The Author(s). Published by the Royal Society of Chemistry

Open Access Article. Published on 23 April 2024. Downloaded on 1/17/2026 12:32:28 AM.
This article is licensed under a Creative Commons Attribution-NonCommercial 3.0 Unported Licence.

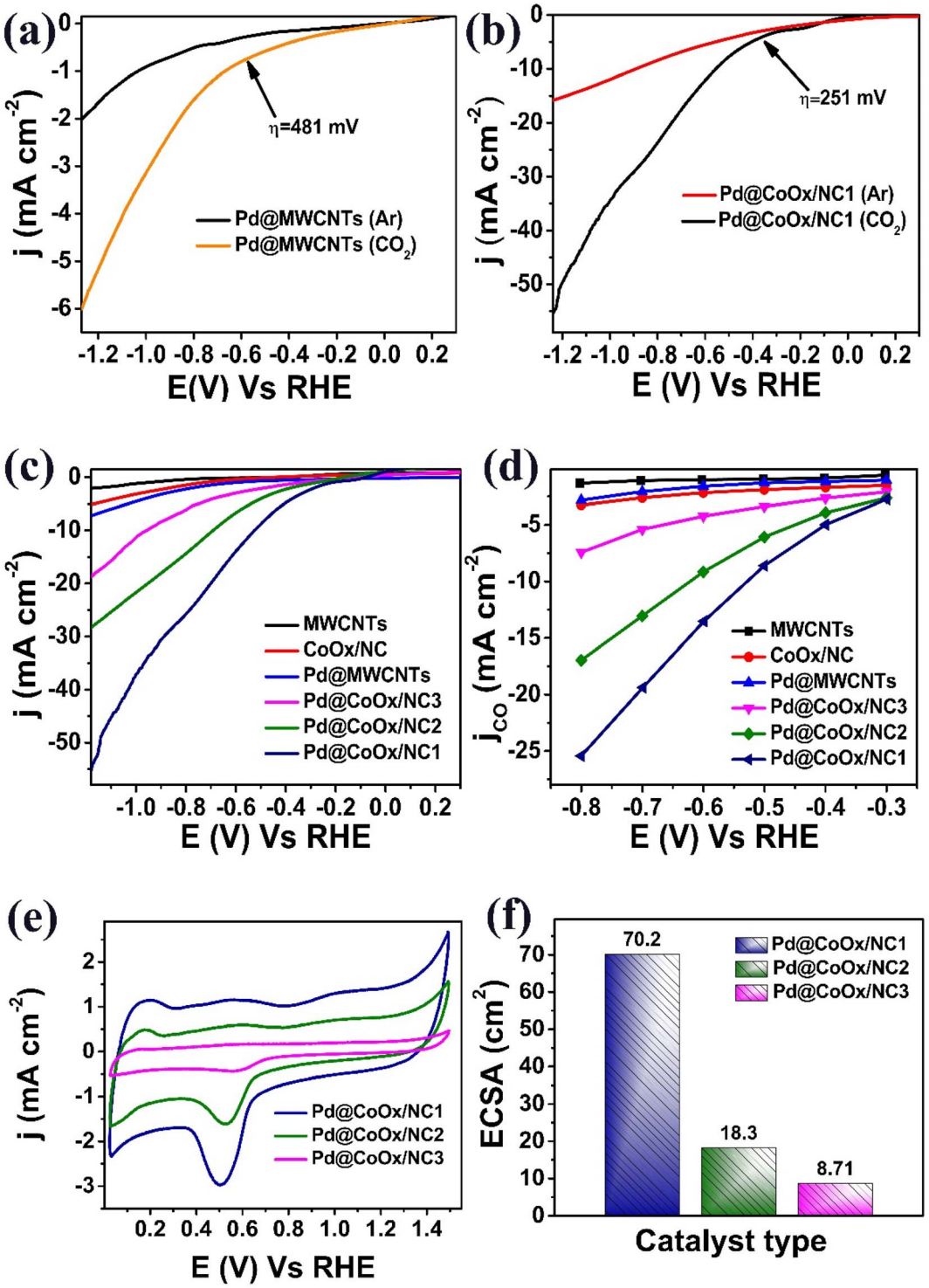

Fig. 3 (a) Comparative LSV analysis of Pd@MWCNTs in Ar and CO_2 environment employing a scan rate of 10 mV s^{-1}, (b) comparative LSV analysis of Pd@CoOx/NC1 in Ar and CO_2 environment employing a scan rate of 10 mV s^{-1}, (c) comparative LSV analysis of all synthesized catalysts in CO_2 saturated medium at 10 mV s^{-1} (d) comparison of partial CO current density of all synthesized electrocatalysts in CO_2 saturated medium at 10 mV s^{-1} (e) CV curves at 1.4 V_{RHE} for oxide layer reduction in Ar saturated medium at 50 mV s^{-1} (f) comparison of the ECSA of the synthesized electrocatalysts.

The electrochemical active surface area (ECSA) of the catalysts was calculated using the Pd–O reduction process by recording cycle voltammetry (CV) curves at 1.4 V_{RHE} as a function of the higher potential limit (Fig. 3e), amongst all the electrocatalysts examined, Pd@CoOx/NC1 showed the largest ECSA (70.2 cm^2) (Fig. 3f). This study highlights the outstanding

© 2024 The Author(s). Published by the Royal Society of Chemistry

Open Access Article. Published on 23 April 2024. Downloaded on 1/17/2026 12:32:28 AM.
This article is licensed under a Creative Commons Attribution-NonCommercial 3.0 Unported Licence.

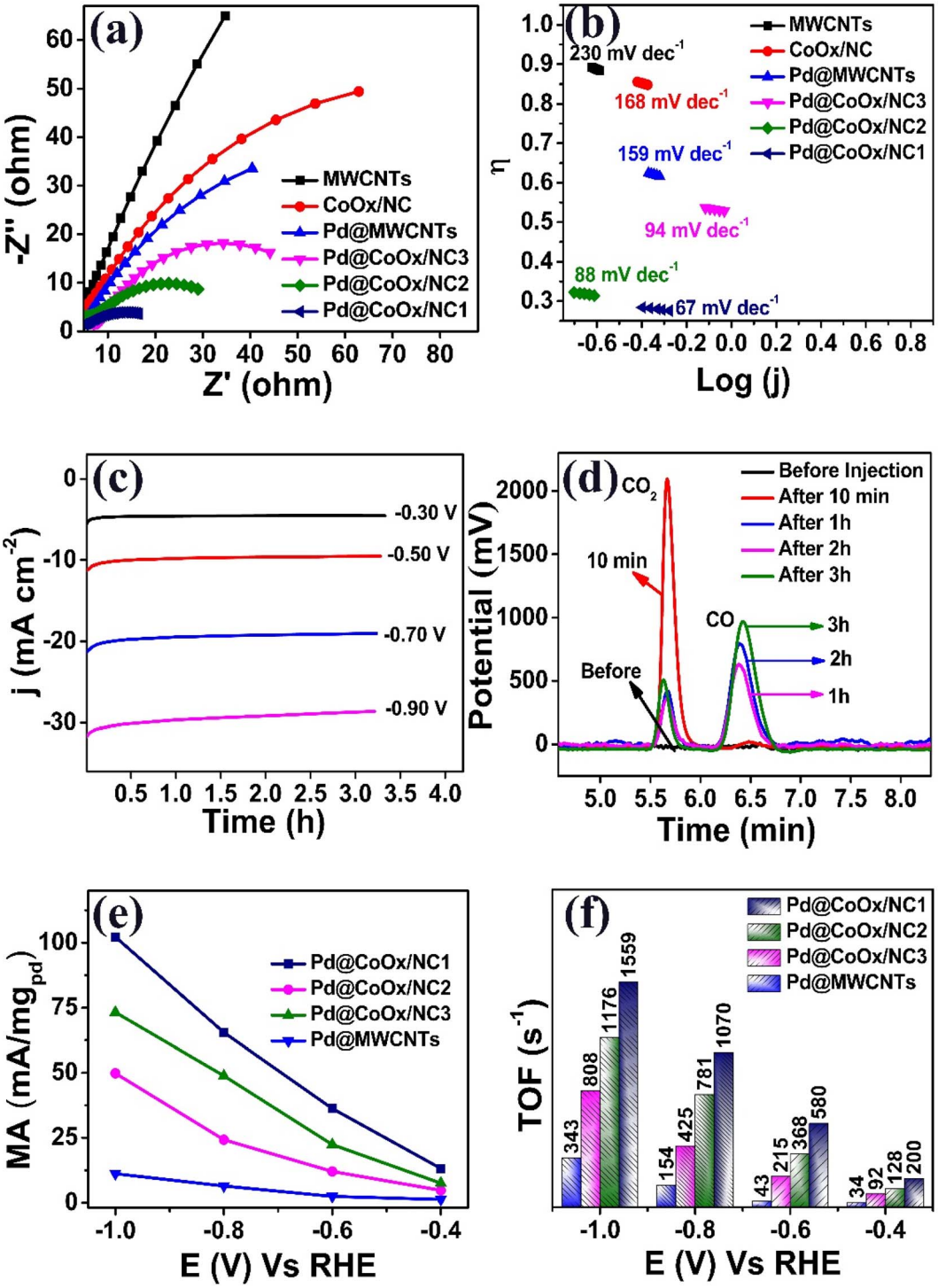

Fig. 4 (a) EIS analysis of all the synthesized catalysts, (b) Tafel slope of all the synthesized electrocatalysts, (c) controlled potential testing of Pd@CoOx/NC1 at various potentials for a time duration of 3.20 h, (d) GC results of CO detection for Pd@CoOx/NC1, (e) comparison of mass activity of all the synthesized electrocatalysts at different potentials, (f) comparison of TOF of Pd@MWCNTs and Pd@CoOx/NCs at different potentials.

electrochemical performance of Pd@CoOx/NC1 due to its greater number of active sites readily available for catalytic processes.

Measurements from electrochemical impedance spectroscopy (EIS) provide important information regarding charge transfer resistance. The Nyquist curve of Pd@CoOx/NC1 showed a substantially smaller semicircular diameter, confirming faster charge transfer conductance and lower charge transfer resistance (Fig. 4a). In comparison to other catalysts, Pd@CoOx/NC1 demonstrates higher reaction efficiency and

© 2024 The Author(s). Published by the Royal Society of Chemistry

Open Access Article. Published on 23 April 2024. Downloaded on 1/17/2026 12:32:28 AM. This article is licensed under a Creative Commons Attribution-NonCommercial 3.0 Unported Licence.

suggests higher catalytic activity for CO_2 reduction. Lower charge transfer resistance, faster electron transfer rates, and a more facile CO_2 reduction pathway are all attributed to the smaller semicircular diameter. Our findings strongly support the outstanding electrocatalytic activity of Pd@CoOx/NC1 and its ability to work as an effective catalyst for eCO_2RR.

The Tafel slope, which gives an idea about the kinetics of the reaction on the surface of an electrode, of all the synthesized electrocatalysts is in the following order. MWCNTs (230 mV dec^{-1}) > CoOx/NC (168 mV dec^{-1}) > Pd@MWCNTs (159 mV dec^{-1}) > Pd@CoOx/NC3 (94 mV dec^{-1}) > Pd@CoOx/NC2 (88 mV dec^{-1}) > Pd@CoOx/NC1 (67 mV dec^{-1}). The lower value of slope indicates better kinetics toward CO_2 reduction reaction (Fig. 4b).

A series of controlled potential electrolysis experiments were conducted at various potentials (from $-0.3V_{RHE}$ to -0.9 V_{RHE}) to evaluate the stability of the highly active catalyst Pd@CoOx/NC1 (Fig. 4c). Remarkably, Pd@CoOx/NC1 exhibited outstanding stability for a time duration of 3.20 h (12 000 s) for each potential test. Throughout this period, there was no discernible degradation in catalytic activity, with only a marginal decrease of approximately 2%. This underscores the catalyst's exceptional long-term performance. The high stability and activity of Pd@CoOx/NC1make it a highly suitable candidate to be employed for eCO_2RR.

A novel qualitative method, the $PdCl_2$ strips technique, was employed to detect the presence of CO gas produced during the eCO_2RR. The method requires 1 N sodium hydroxide, 0.1 N hydrochloric acid, 0.5 N palladium chloride solution, and filter paper. To prepare the $PdCl_2$ strips, a longitudinal strip of filter paper measuring 3 cm × 1 cm is immersed in a 0.5 N $PdCl_2$ solution prepared in 0.1 N HCl and allowed to air dry. Subsequently, 1–2 drops of 1.0 N NaOH are applied to the strip. The prepared strip is then suspended in the cathodic chamber's headspace. As the reaction progresses, the CO produced changes the color of the strip from colorless to black, indicating the interaction with $PdCl_2$. This change in color serves as confirmation of CO production (Fig. S7†).

For the quantitative determination of CO, gas chromatography (GC) analysis was employed. Under controlled potential conditions (−0.7 V *vs.* RHE) of 3 h, the FE of the optimized electrocatalyst *i.e.*, Pd@CoOx/NC1, was evaluated. At hourly intervals, gaseous samples were taken and analyzed by GC. The resulting chromatogram, shown in (Fig. 4d), provides a thorough picture of how the gas composition changed throughout the reaction. These results highlight the efficiency of Pd@CoOx/NC1 as a catalyst for CO_2 reduction processes by providing useful insights into its selectivity and catalytic performance. The outstanding electrocatalytic activity of Pd@CoOx/NC1 in selectively converting CO_2 to CO was demonstrated by the FE_{CO} of 81%.

The contribution of other liquid electrocatalytic reduced products in faradaic efficiency was evaluated using head space gas chromatographic with flame ionization detector (HS-GCFID). The sensitivity of instrument and method verification was done using positive control. Notably, in the positive control, a peak at a retention time (R_t) of 6.8 min confirmed the presence of formic acid. However, it is noteworthy that no such peak was observed at the same R_t during the catalytic activity, thus excluding the formation of formic acid (Fig. S8†).

Table 1 Comparison of the Pd-based electrocatalysts work with the reported literature

Catalysts	V *vs.* RHE	FE%	References
Pd@CoOx/NC1	−0.70	81	This work
$Pd_{2.4nm}$	−0.89	91.2	10
Pd foil	−0.80	28	17
Pd/C	−0.60	40	18
$Pd_{85}Cu_{15}$/C	−0.89	86	28
Pd_7Cu_3	−0.80	80	41
Pd@Cu_2O-2	−0.77	58.3	42
Pd_5@Au_{95}	−0.5	∼80	43
$PdAg_3$	−0.8	96.2	44
Pd_2 DAC	−0.85	98.2	45
Pd nanosheets	−0.5	94	46
Pd icosahedra/C	−0.8	91.1	47
4.3 Pd–SnO_2	−1.1	78.6	48

Moreover, the determination of other liquid products, such as methanol, ethanol, propanol, and isopropanol, was undertaken utilizing HS-GCFID. Standards for all potential products were run alongside an internal standard (IS) acetone (Fig. S9a†). Upon analysis at various time intervals, solely the peak of the IS was detected, with no evidence of any other products (Fig. S9b†). This observation underscores the selectivity of our catalyst toward CO, thus affirming its efficiency in CO selectivity.

The mass activities (mA/mg_{pd}) of the synthesized electrocatalysts were calculated at different potentials from -0.4 V_{RHE} to -1.0 V_{RHE}. The mass activities of all the electrocatalysts, highlighting their respective performance in the electrocatalytic CO_2 to CO conversion process, were observed in the following sequence. Pd@MWCNTs < Pd@CoOx/NC3 < Pd@CoOx/NC2 < Pd@CoOx/NC1(Fig. 4(e)).

Furthermore, turnover frequency (TOF) was calculated at different potentials from -0.4 V_{RHE} to -1.0 V_{RHE} in a CO_2 saturated medium. The TOF of Pd@CoOx/NC1 is (1559 s^{-1}) at -1.0 V_{RHE} which is 4.54, 1.93 and 1.33 times higher than Pd@MWCNTs (343 s^{-1}), Pd@CoOx/NC3 (808 s^{-1}) and Pd@CoOx/NC2 (1176 s^{-1}), respectively. The higher TOF value of Pd@CoOx/NC1 indicates a faster rate of catalytic reaction (Fig. 4f). The comparison of Pd-based electrocatalysts with the recent literature has been shown in Table 1.

Conclusions

A facile synthesis route was employed to prepare a series of Pd@CoOx/NCs electrocatalysts for CO_2 reduction reactions. In particular, the catalyst Pd@CoOx/NC1 exhibited a remarkable FE of about 81% for CO production, as confirmed by GC-TCD analysis. These findings are qualitatively supported by our innovative $PdCl_2$ strip detection method. Importantly, Pd@CoOx/NC1 shows a high current density of 55 mA cm^{-2} and a remarkably low overpotential of 251 mV, demonstrating its efficiency in promoting CO_2 reduction. The catalyst exhibited great stability at various potentials, and the Nyquist plot showed

© 2024 The Author(s). Published by the Royal Society of Chemistry

Open Access Article. Published on 23 April 2024. Downloaded on 1/17/2026 12:32:28 AM. This article is licensed under a Creative Commons Attribution-NonCommercial 3.0 Unported Licence.

a lower semicircle, indicating enhanced charge transfer kinetics. The outstanding performance, selectivity, and stability of Pd@CoOx/NC1's make it an important material that could contribute towards renewable energy technologies.

Conflicts of interest

There are no conflicts to declare.

Acknowledgements

The work was financially supported by the Pakistan Academy of Sciences (PAS) and Higher Education Commission (HEC) of Pakistan (No. 8400/Federal/NRPU/R&D/HEC/2017).

References

1 C.-W. Kung, C. O. Audu, A. W. Peters, H. Noh, O. K. Farha and J. T. Hupp, Copper nanoparticles installed in metal–organic framework thin films are electrocatalytically competent for CO_2 reduction, *ACS Energy Lett.*, 2017, **2**(10), 2394–2401.

2 F. Nasim and M. A. Nadeem, Understanding the mechanism and synergistic interaction of cobalt-based electrocatalysts containing nitrogen-doped carbon for 4 e^- ORR, *J. Mater. Chem. A*, 2023, **11**(19), 10095–10124.

3 F. Nasim, H. Ali, M. A. Nadeem and M. A. Nadeem, High-performance FeOx@CoOx/NC electrocatalysts for the oxygen reduction reaction in alkaline media, *Sustainable Energy Fuels*, 2023, **7**(1), 190–200.

4 F. Nasim, H. Ali, A. Waseem, M. A. Nadeem and M. A. Nadeem, Confinement of CoOx-CoP nanoparticles inside nitrogen doped CNTs: A low-cost ORR electrocatalyst, *Int. J. Hydrogen Energy*, 2022, **47**(94), 39898–39907.

5 J. M. Hall-Spencer, R. Rodolfo-Metalpa, S. Martin, E. Ransome, M. Fine, S. M. Turner, S. J. Rowley, D. Tedesco and M.-C. Buia, Volcanic carbon dioxide vents show ecosystem effects of ocean acidification, *Nature*, 2008, **454**(7200), 96–99.

6 S. J. Davis, K. Caldeira and H. D. Matthews, Future CO_2 emissions and climate change from existing energy infrastructure, *J. Sci.*, 2010, **329**(5997), 1330–1333.

7 G. A. Olah, G. S. Prakash and A. Goeppert, Anthropogenic chemical carbon cycle for a sustainable future, *J. Am. Chem. Soc.*, 2011, **133**(33), 12881–12898.

8 E. V. Kondratenko, G. Mul, J. Baltrusaitis, G. O. Larrazábal and J. Pérez-Ramírez, Status and perspectives of CO_2 conversion into fuels and chemicals by catalytic, photocatalytic and electrocatalytic processes, *Energy Environ. Sci.*, 2013, **6**(11), 3112–3135.

9 M. Aresta, A. Dibenedetto and A. Angelini, Catalysis for the valorization of exhaust carbon: from CO_2 to chemicals, materials, and fuels. Technological use of CO_2, *Chem. Rev.*, 2014, **114**(3), 1709–1742.

10 D. Gao, H. Zhou, J. Wang, S. Miao, F. Yang, G. Wang, J. Wang and X. Bao, Size-dependent electrocatalytic reduction of CO_2 over Pd nanoparticles, *J. Am. Chem. Soc.*, 2015, **137**(13), 4288–4291.

11 M. Liu, J. Balamurugan, T. Liang and C. Liu, Theoretical study of β12 borophene supported metal for electrocatalytic CO_2 reduction reaction, *Appl. Surf. Sci.*, 2024, **642**, 158594.

12 M. Liu, J. Balamurugan, T. Liang and C. Liu, Mechanism of electrocatalytic CO_2 reduction reaction by borophene supported bimetallic catalysts, *J. Colloid Interface Sci.*, 2024, **659**, 959–973.

13 D. T. Whipple and P. J. Kenis, Prospects of CO_2 utilization *via* direct heterogeneous electrochemical reduction, *J. Phys. Chem. Lett.*, 2010, **1**(24), 3451–3458.

14 J. Qiao, Y. Liu, F. Hong and J. Zhang, A review of catalysts for the electroreduction of carbon dioxide to produce low-carbon fuels, *Chem. Soc. Rev.*, 2014, **43**(2), 631–675.

15 Y. Zhao, X. Tan, W. Yang, C. Jia, X. Chen, W. Ren, S. C. Smith and C. Zhao, Surface reconstruction of ultrathin palladium nanosheets during electrocatalytic CO_2 reduction, *Angew. Chem., Int. Ed.*, 2020, **59**(48), 21493–21498.

16 Y. Peng, M. Cui, Z. Zhang, S. Shu, X. Shi, J. T. Brosnahan, C. Liu, Y. Zhang, P. Godbold and X. Zhang, Bimetallic composition-promoted electrocatalytic hydrodechlorination reaction on silver–palladium alloy nanoparticles, *ACS Catal.*, 2019, **9**(12), 10803–10811.

17 Y. Hori, H. Wakebe, T. Tsukamoto and O. Koga, *Electrochim. Acta*, 1994, **39**(11–12), 1833–1839.

18 W. Sheng, S. Kattel, S. Yao, B. Yan, Z. Liang, C. J. Hawxhurst, Q. Wu and J. G. Chen, Electrochemical reduction of CO_2 to synthesis gas with controlled CO/H_2 ratios, *Energy Environ. Sci.*, 2017, **10**(5), 1180–1185.

19 D. Gao, H. Zhou, F. Cai, J. Wang, G. Wang and X. Bao, Pd-containing nanostructures for electrochemical CO_2 reduction reaction, *ACS Catal.*, 2018, **8**(2), 1510–1519.

20 B. A. Rosen, A. Salehi-Khojin, M. R. Thorson, W. Zhu, D. T. Whipple, P. J. Kenis and R. I. Masel, Ionic liquid–mediated selective conversion of CO_2 to CO at low overpotentials, *J. Sci.*, 2011, **334**(6056), 643–644.

21 C. E. Tornow, M. R. Thorson, S. Ma, A. A. Gewirth and P. J. Kenis, Nitrogen-based catalysts for the electrochemical reduction of CO_2 to CO, *J. Am. Chem. Soc.*, 2012, **134**(48), 19520–19523.

22 S. Zhang, P. Kang, S. Ubnoske, M. K. Brennaman, N. Song, R. L. House, J. T. Glass and T. J. Meyer, Polyethylenimine-enhanced electrocatalytic reduction of CO_2 to formate at nitrogen-doped carbon nanomaterials, *J. Am. Chem. Soc.*, 2014, **136**(22), 7845–7848.

23 Y. Chen and M. W. Kanan, Tin oxide dependence of the CO_2 reduction efficiency on tin electrodes and enhanced activity for tin/tin oxide thin-film catalysts, *J. Am. Chem. Soc.*, 2012, **134**(4), 1986–1989.

24 Q. Lu, J. Rosen, Y. Zhou, G. S. Hutchings, Y. C. Kimmel, J. G. Chen and F. Jiao, A selective and efficient electrocatalyst for carbon dioxide reduction, *Nat. Commun.*, 2014, **5**(1), 3242.

25 A. A. Peterson, F. Abild-Pedersen, F. Studt, J. Rossmeisl and J. K. Nørskov, How copper catalyzes the electroreduction of

Open Access Article. Published on 23 April 2024. Downloaded on 1/17/2026 12:32:28 AM. This article is licensed under a Creative Commons Attribution-NonCommercial 3.0 Unported Licence.

carbon dioxide into hydrocarbon fuels, *Energy Environ. Sci.*, 2010, **3**(9), 1311–1315.

26 R. Kas, R. Kortlever, A. Milbrat, M. T. Koper, G. Mul and J. Baltrusaitis, Electrochemical CO_2 reduction on Cu_2O-derived copper nanoparticles: controlling the catalytic selectivity of hydrocarbons, *J. Chem. Phys.*, 2014, **16**(24), 12194–12201.

27 M. Cui, G. Johnson, Z. Zhang, S. Li, S. Hwang, X. Zhang and S. Zhang, AgPd nanoparticles for electrocatalytic CO_2 reduction: bimetallic composition-dependent ligand and ensemble effects, *Nanoscale*, 2020, **12**(26), 14068–14075.

28 Z. Yin, D. Gao, S. Yao, B. Zhao, F. Cai, L. Lin, P. Tang, P. Zhai, G. Wang and D. Ma, Highly selective palladium-copper bimetallic electrocatalysts for the electrochemical reduction of CO_2 to CO, *Nano Energy*, 2016, **27**, 35–43.

29 F. Zulfiqar, A. Hameed, A. Shahzad, S. S. A. Shah and M. A. Nadeem, Pronounced effect of phosphidization on the performance of CoOx encapsulated N-doped carbon nanotubes towards oxygen evolution reaction, *Int. J. Hydrogen Energy*, 2022, **47**(52), 22054–22062.

30 F. Nasim, H. Ali and M. A. Nadeem, The pronounced effect of cobalt oxide on the electrocatalytic activity of palladium nanoparticles anchored on CoOx/NC towards the ORR with increased MA and ECSA, *Mater. Adv.*, 2023, **4**(2), 578–585.

31 X. Chen, D.-D. Ma, B. Chen, K. Zhang, R. Zou, X.-T. Wu and Q.-L. Zhu, Metal–organic framework-derived mesoporous carbon nanoframes embedded with atomically dispersed Fe–Nx active sites for efficient bifunctional oxygen and carbon dioxide electroreduction, *Appl. Catal., B*, 2020, **267**, 118720.

32 M. Xie, J. Wang, X.-L. Du, N. Gao, T. Liu, Z. Li, G. Xiao, T. Li and J.-Q. Wang, Metal–organic framework derived single-atom catalysts for electrochemical CO_2 reduction, *RSC Adv.*, 2022, **12**(50), 32518–32525.

33 C. Jia, W. Ren, X. Chen, W. Yang, C. Zhao and B. N, Dual heteroatom-doped hierarchical porous carbon framework for efficient electroreduction of carbon dioxide, *ACS Sustain. Chem. Eng.*, 2020, **8**(15), 6003–6010.

34 X. Liang, N. Tian, Z. Zhou and S. Sun, N, P dual-doped porous carbon nanosheets for high-efficiency CO_2 electroreduction, *ACS Sustain. Chem. Eng.*, 2022, **10**(5), 1880–1887.

35 P. P. Sharma, J. Wu, R. M. Yadav, M. Liu, C. J. Wright, C. S. Tiwary, B. I. Yakobson, J. Lou, P. M. Ajayan and X. D. Zhou, Nitrogen-doped carbon nanotube arrays for high-efficiency electrochemical reduction of CO_2: on the understanding of defects, defect density, and selectivity, *Angew. Chem., Int. Ed. Engl.*, 2015, **127**(46), 13905–13909.

36 D. Wang, J. Mao, C. Zhang, J. Zhang, J. Li, Y. Zhang and Y. Zhu, Modulating Microenvironments to Enhance CO_2 Electroreduction Performance, *eScience*, 2023, 100119.

37 K. S. Park, Z. Ni, A. P. Côté, J. Y. Choi, R. Huang, F. J. Uribe-Romo, H. K. Chae, M. O'Keeffe and O. M. Yaghi, Exceptional chemical and thermal stability of zeolitic imidazolate frameworks, *Proc. Natl. Acad. Sci. U.S.A.*, 2006, **103**(27), 10186–10191.

38 I. Khan, F. Nasim, M. Choucair, S. Ullah, A. Badshah and M. Nadeem, Cobalt oxide nanoparticle embedded N-CNTs: lithium ion battery applications, *RSC Adv.*, 2016, **6**(2), 1129–1135.

39 S. Mondal and C. R. Raj, Electrochemical dealloying-assisted surface-engineered Pd-based bifunctional electrocatalyst for formic acid oxidation and oxygen reduction, *ACS Appl. Mater. Interfaces*, 2019, **11**(15), 14110–14119.

40 C. Goswami, H. Saikia, K. Tada, S. Tanaka, P. Sudarsanam, S. K. Bhargava and P. Bharali, Bimetallic palladium–nickel nanoparticles anchored on carbon as high-performance electrocatalysts for oxygen reduction and formic acid oxidation reactions, *ACS Appl. Energy Mater.*, 2020, **3**(9), 9285–9295.

41 M. Li, J. Wang, P. Li, K. Chang, C. Li, T. Wang, B. Jiang, H. Zhang, H. Liu and Y. Yamauchi, Mesoporous palladium–copper bimetallic electrodes for selective electrocatalytic reduction of aqueous CO_2 to CO, *J. Mater. Chem.*, 2016, **4**(13), 4776–4782.

42 R. Cai, X. Du, G. Liu, X. Wang, Q. Tang, X. Pan, F. Li and J. Li, Controllable Pd@ Cu_2O Schottky junction interface with improved anti-poisoning effect for efficiently electroreduction of CO_2 into syngas, *J. Fuels*, 2023, **338**, 127346.

43 Y. Wang, L. Cao, N. J. Libretto, X. Li, C. Li, Y. Wan, C. He, J. Lee, J. Gregg and H. Zong, Ensemble effect in bimetallic electrocatalysts for CO_2 reduction, *J. Am. Chem. Soc.*, 2019, **141**(42), 16635–16642.

44 T. Gunji, H. Ochiai, T. Ohira, Y. Liu, Y. Nakajima and F. Matsumoto, Preparation of various Pd-based alloys for electrocatalytic CO_2 reduction reaction—selectivity depending on secondary elements, *Chem. Mater. Chem.*, 2020, **32**(16), 6855–6863.

45 N. Zhang, X. Zhang, Y. Kang, C. Ye, R. Jin, H. Yan, R. Lin, J. Yang, Q. Xu and Y. Wang, A supported Pd_2 dual-atom site catalyst for efficient electrochemical CO_2 reduction, *Angew. Chem., Int. Ed. Engl.*, 2021, **133**(24), 13500–13505.

46 W. Zhu, L. Zhang, P. Yang, C. Hu, Z. Luo, X. Chang, Z. J. Zhao and J. Gong, Low-coordinated edge sites on ultrathin palladium nanosheets boost carbon dioxide electroreduction performance, *Angew. Chem., Int. Ed. Engl.*, 2018, **57**(36), 11544–11548.

47 H. Huang, H. Jia, Z. Liu, P. Gao, J. Zhao, Z. Luo, J. Yang and J. Zeng, Understanding of strain effects in the electrochemical reduction of CO_2: using Pd nanostructures as an ideal platform, *Angew. Chem., Int. Ed. Engl.*, 2017, **129**(13), 3648–3652.

48 H. He, D. Xia, X. Yu, J. Wu, Y. Wang, L. Wang, L. Wu, J. Huang, N. Zhao and L. Deng, Pd-SnO_2 interface enables synthesis of syngas with controllable H_2/CO ratios by electrocatalytic reduction of CO_2, *Appl. Catal., B*, 2022, **312**, 121392.

© 2024 The Author(s). Published by the Royal Society of Chemistry